Energies **2015**, *8*, 3272-3291; doi:10.3390/en8043272

OPEN ACCESS

energies

ISSN 1996-1073

www.mdpi.com/journal/energies

Article

Nearshore Tests of the Tidal Compensation System for Point-Absorbing Wave Energy Converters

Valeria Castellucci *, Johan Abrahamsson, Tobias Kamf and Rafael Waters

Swedish Centre for Renewable Electric Energy Conversion, Division for Electricity, Uppsala University, Box 534, Uppsala 751 21, Sweden;
E-Mails: johan.abrahamsson@angstrom.uu.se (J.A.); tobias.kamf@angstrom.uu.se (T.K.); rafael.waters@angstrom.uu.se (R.W.)

* Author to whom correspondence should be addressed; E-Mail: valeria.castellucci@angstrom.uu.se; Tel.: +46-18-4715843; Fax: +46-18-4715810.

Academic Editor: John Ringwood

Received: 16 February 2015 / Accepted: 3 April 2015 / Published: 22 April 2015

Abstract: The power production of the linear generator wave energy converter developed at Uppsala University is affected by variations of mean sea level. The reason is that these variations change the distance between the point absorber located on the surface and the linear generator located on the seabed. This shifts the average position of the translator with respect to the center of the stator, thereby reducing the generator output power. A device mounted on the point absorber that compensates for tides of small range by regulating the length of the connection line between the buoy at the surface and the linear generator has been constructed and tested. This paper describes the electro-mechanical, measurement, communication and control systems installed on the buoy and shows the results obtained before its connection to the generator. The adjustment of the line was achieved through a linear actuator, which shortens the line during low tides and *vice versa*. The motor that drives the mechanical device was activated remotely via SMS. The measurement system that was mounted on the buoy consisted of current and voltage sensors, accelerometers, strain gauges and inductive and laser sensors. The data collected were transferred via Internet to a Dropbox server. As described within the paper, after the calibration of the sensors, the buoy was assembled and tested in the waters of Lysekil harbor, a few kilometers from the Uppsala University research site. Moreover, the performance of the sensors, the motion of the mechanical device, the power consumption, the current control strategy and the communication system are discussed.

Keywords: wave energy; tidal compensation; nearshore tests; measurement technique

1. Introduction

The wave energy concept developed by Uppsala University comprises a directly-driven linear generator placed on the seabed and connected with a point-absorber buoy floating on the surface via a connection line. The heave motion of the buoy causes a translator to move within a stator, inducing electrical power [1]. The energy absorption (and thereby, power output) for the current design of the studied wave energy converter (WEC) decreases when the water level deviates from its average by more than ± 20 cm [2], e.g., due to tides. The reason is that the average position of the translator is no longer centered with respect to the stator.

The WECs tested at the Lysekil research site perform fairly well due to the modest tidal range that characterizes the Swedish west coast [3–6]. However, it is necessary to handle mean sea level variations in order for this technology to be suitable for other seas and oceans where the tides are more significant. As one of the possible solutions to this end, a mechanical device able to adjust the length of the connection line has been mounted on a buoy. This device is able to compensate for small sea water level variations, typically 1 m in amplitude [7]. The mechanical system was equipped with measurement and control systems, which monitor and remotely activate the device.

The goal of a compensation system for sea level variations is not only to optimize the power output of the generator during tides, but also to compensate for the error due to misalignment of the center of the stator with the center of the translator during deployment [8]. Misalignment may be caused by inaccurate calculation of the depth at the site and/or miscalculation of the translator position when the buoy is connected to the line. The average depth at the site determines how long the line between the translator and the buoy should be. The measurement of average depth is typically influenced by the instantaneous tidal level.

A third benefit of a compensation system is the ease of deployment. Typically, the buoy is attached to the connection line by divers that need to lift the translator with air bags during the deployment. The volume of air necessary to lift the translator in order to center it with respect to the stator is calculated knowing the weight of the translator. Moreover, the divers measure the difference between the position of the translator when resting on the bottom of the generator and the position when lifted with the air bags. The difference should be equal to half of the stroke length. Once the right position is reached, the divers connect the line to the buoy. This process is time consuming, hence expensive. The compensation system would drastically reduce the underwater work and would make the operations safer for the divers.

This paper describes in detail the mechanical, electrical and measurement systems installed on a toroidal buoy, which was used in 2009 to run tests on a generator named L9 and which was recently refurbished to carry out this experiment. Moreover, the paper shows the nearshore results obtained before the deployment and connection to the generator.

2. Experimental Setup

This chapter describes the different components of the compensation system, according to the schematic illustrated in Figure 1.

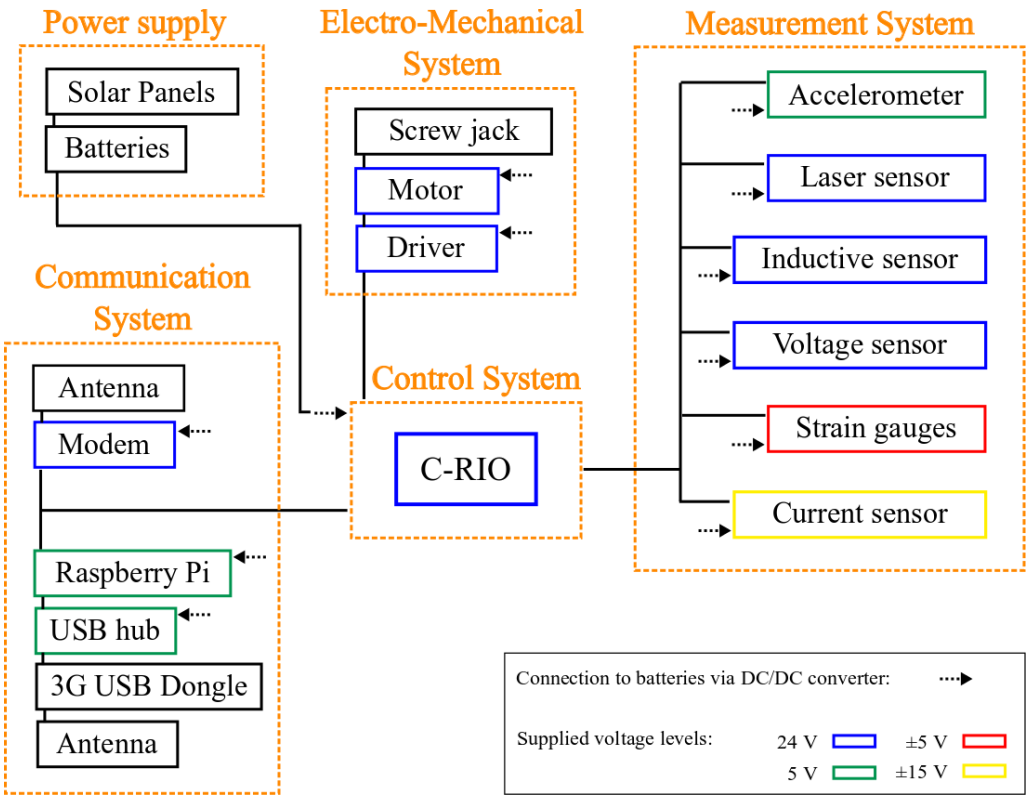

Figure 1. Schematic of the systems installed inside the buoy.

2.1. Power Supply

The power supply for the entire system consisted of two 12 V batteries, each with a capacity of 100 Ah, connected in series. The batteries were charged by four solar panels. The various components of the system were connected to the batteries via suitable voltage level DC/DC converters.

Four CT30 SolarMarine solar panels were chosen, each having a nominal voltage of 12 V and a nominal power of 30 W [9]. To match the voltage required by the batteries, the panels were separated into two pairs, which were connected in series. The pairs were thereafter connected in parallel, yielding a system with a nominal voltage of 24 V and a nominal power of 120 W.

One solar charge controller [10] regulated the charge flowing from the solar panels to the batteries, as well as providing current to the load. The regulator used pulse width-modulated (PWM) charging of the batteries and was rated at 240 W. The regulator featured overvoltage protection during charging, as well as deep-discharge protection by load shedding.

Figure 2 shows measurements of battery voltage over time during the summer season, as well as the autumn season. The electro-mechanical system was turned off in both cases, while the control, communication and measurement systems were active; hence, the consumption was about 15 W.

The green curve shows the behavior of the battery voltage during four typical summer days, while the blue curve shows the charge during four typical autumn days.

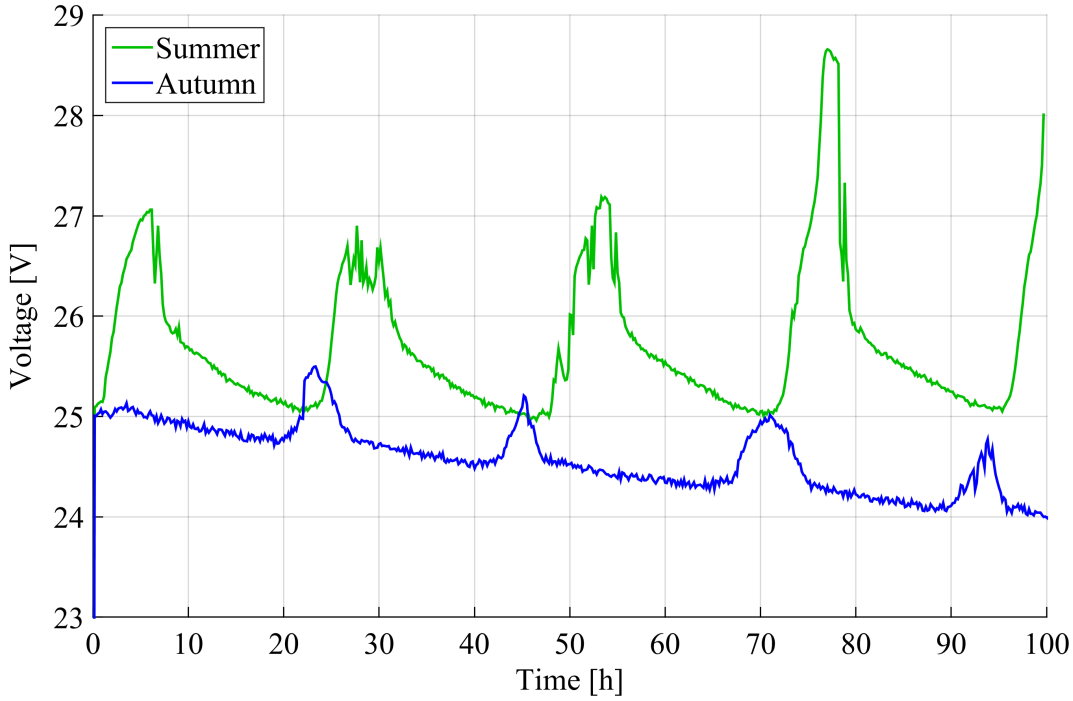

Figure 2. Charging of batteries by the solar panels. The green curve displays the battery voltage during a time-period of four days in the summer. The blue curve is the corresponding measurement during autumn.

In the first case, the batteries discharged during the night, but were fully charged by the Sun during the day. In the second case, the sunlight was not strong enough to fully charge the batteries, and the tendency of the battery was to slowly discharge.

One important advantage of using a regulator is the following: if the battery charge decreases below a certain minimum level, in this case 22.2 V, the load turns off and waits until the batteries have reached a voltage of 26.2 V before restarting. This feature ensured that the batteries would not suffer permanent damage from deep discharge during times with little or no sunlight. The results show that this is a mandatory feature during the Swedish winter, unless more solar panels were to be installed. In the latter case, this would become just a precautionary feature.

2.2. Electro-Mechanical System

The electro-mechanical system consisted of a screw jack connected to the steel wire, which joins the buoy to the generator, the so-called connection line. The screw moved up or down when required, in order to reduce or increase the length of the connection line, respectively. This solution, adopted for small tidal ranges, was demonstrated to be self-locking, *i.e.*, the screw keeps its position without unscrewing, for all of the operational loads [7].

The screw jack was mechanically designed for the generator L9, a rare-earth permanent magnet generator, comprising a lighter translator compared with the new ferrite generators [11]. The maximum tension in the wire that connects the buoy to the L9 can reach 300 kN approximately, and the weight of the translator is 2700 kg [12]. For this reason, the device was dimensioned to hold a peak force of 300 kN and to be able to lift 30 kN [13].

The chosen M80 screw had trapezoidal treads and was 2 m long. As shown in Figure 3, the screw ran into a nut, which was linked to a worm screw via a worm wheel. The worm screw was locked to the shaft of a motor via a flexible joint to avoid the negative effects of possible misalignments. The screw and the worm were made of steel, while the nut was made of brass: the steel has high mechanical strength, and the brass has good resistance to corrosion and a low friction coefficient in the coupling screw-nut. Moreover, the brass allows the threads to deform so that high loads can be better distributed.

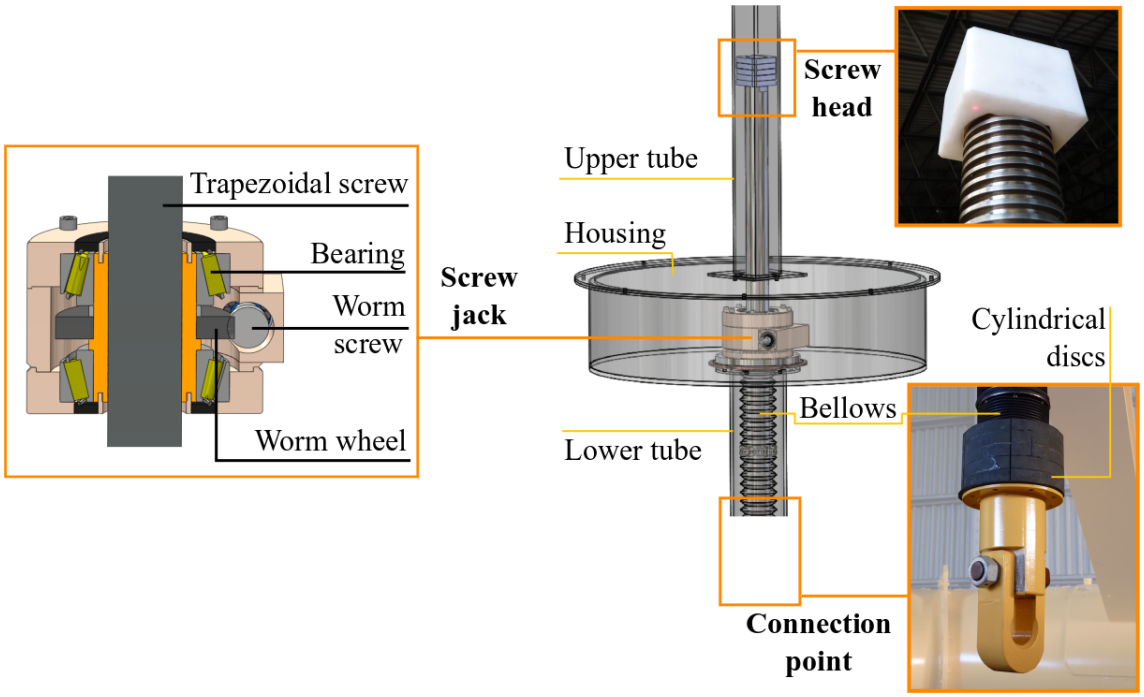

Figure 3. Drawing of the mechanical device. From the top right, the screw head slides into a tube with a square cross-section; the screw jack is protected inside a steel housing that will contain the control and measurement systems, as well; the lower part of the screw is fitted with bellows to avoid contact with water and slides into a round cross-section tube; the lowest part of the screw terminates with a socket that is connected to the line down to generator.

The nut was supported by two bearings, enabling it to rotate relatively to the buoy, while the screw was supposed to move only in the vertical direction. In reality, the screw tended to rotate with the nut due to the high friction between the treads. This was solved by fixing a square plastic element at one end of the screw: this component slid vertically inside a tube of a square cross-section, as shown in Figure 3. Hence, the screw did not experience any rotation. Moreover, this white element worked as a target for the laser sensor, which will be described in Section 2.5.

Even though the buoy moves mostly in heave, it also experiences translations and rotations in different directions, and the screw has to accommodate these movements. This means that the screw will not only experience a normal force, but also a radial force that can damage the device. In order to prevent the system from breaking, a series of circular plastic elements were locked at the bottom of the screw. These discs ran along the circular lower tube, visible in Figure 3, and they transferred the radial force to the beams mounted on the buoy.

Further, the sensitive components, e.g., the motor, the batteries and the sensors, were protected from water infiltration by the housing shown in Figure 3. In order to isolate the lower part of the screw from the water, rubber bellows were used: they stretch or compress according to the direction of motion of the screw.

The DC-motor chosen to drive the screw jack was produced by the company Drive Systems (LN70.5) and had a rated voltage of 24 V, a rated speed of 3.000 r/min and a rated power of 320 W. The standard planetary gear EP 90/1C from the company Tramec with a gear ratio of 1:10 was connected between the shaft of the motor and the screw jack.

A DC-DC converter, used as a buck-converter, was used to control the current to the DC-motor, using pulse width modulation (PWM). The converter was custom made for the application, using two insulated-gate bipolar transistor (IGBT) modules rated at 200 A and 600 V from Fuji Electric (2MB1200U2A-060-50). The IGBT-modules were heavily over-dimensioned for the DC motor, in order to ensure reliability. Two dual-channel driver cores were used to generate the PWM signals needed to switch the four IGBTs. The cores were purchased from Concept (2SC0108T2A0-17), rated for usage with IGBT modules up to 600 A and 1.2 kV and used in complementary mode.

2.3. Control System

The heart of the control system was a programmable automation controller (PAC) from National Instruments, the CompactRIO (cRIO-9076). The PAC combines an industrial real-time controller (400 MHz) and a reconfigurable field-programmable gate array (FPGA) chip, the Spartan-6 LX45 from Xilinx, inside a rugged chassis with four slots containing reconfigurable analog-to-digital converters for machine control and monitoring applications.

Two slots were used in this application: the first to collect analog inputs from the measurement sensors and the second to send digital outputs (PWM signals) to the motor driver. For these purposes, the NI 9205 Analog Input module and the NI 9401 TTL Digital I/O module were used, respectively.

Further, the cRIO comprised: an RS-232 serial port, which was connected to a Global System for Mobile Communications (GSM) modem to exchange SMS; an Ethernet port, used to transfer files via File Transfer Protocol (FTP) to a Raspberry Pi microcomputer; a USB port, which was connected to a USB stick to store data in case of communication failure. Figure 1 illustrates which components were connected to the cRIO, and a detailed description of those will follow below.

2.4. Communication System

The command that activated the linear actuator was encoded as a short message, SMS, and sent from the mainland to the buoy. The message was received by the modem Fargo Maestro 100 GSM/GPRS

900/1800. This model is now considered outdated; hence, it was less expensive, but still good for this application [14].

Moreover, the Raspberry Pi (RPi), a low-cost single-board computer, was connected to the cRIO via Ethernet port and used to retrieve data from the FTP server of the cRIO. Typically, the RPi model B consumes from 0.7 A to 1 A depending on which peripherals are connected, and it was supplied with 5 V [15].

In order to provide the RPi with an Internet connection, a USB dongle Huawei E3131 was plugged into the RPi via a USB hub with external power supply. The reason why a hub was used was that the USB dongle required more power than the RPi could deliver.

The use of a second modem is justified, firstly by the fact that it is safer to have redundancy in the system and, secondly, because the measurement data transfer will not be a necessary feature for a future control system. Hence, the second modem could be removed without compromising the basic control strategy.

2.5. Measurement System

As illustrated in Figure 1, different kinds of sensors were mounted on the buoy. A description of each of them is given below.

The accelerometer chosen for this application was the DE-ACCM3D, which measures acceleration in 3 axes in the range of ± 3 g [16]. The sensor provided information on the buoy motion in all directions. The position of the buoy was valuable information for *a posteriori* analyses of the behavior of the system.

A distance sensor was installed with the purpose of monitoring the position of the connection line, which would vary approximately 1 m, given the mean sea level variation range at the Lysekil research site. The sensor would provide information on the correct operation of the mechanical adjustment device. To this end, a laser sensor from Micro Epsilon (optoNCDT ILR 1030-8) was selected. It is a compact sensor that can measure distances in the range from 0.2 m to 2 m with a spot diameter of a few millimeters. The price-performance ratio of the sensor was considered good and the resolution of the measurement and the bandwidth high enough (1 mm, 100 Hz) [17].

With the purpose of calculating the revolutions of the shaft of the motor during the adjustment of the connection line, an inductive sensor from CONTRINEX (DW-AD-509-M18) was used [18]. According to the specifications, the inductive sensor had a sensing range from 0 mm to 10 mm and was installed to face the shaft where two teeth made of conductive materials were mounted.

The battery voltage was measured with the help of a simple voltage divider, which consisted of three series-connected resistors (10 kΩ) mounted on the battery poles. The typical battery voltage being from 21 V to 28 V and the input range of the analog input of the cRIO 10 V, the necessity for a voltage divider is self-explanatory.

In order to measure deformations on the buoy and, hence, to calculate the forces that the screw had to endure, three active strain gauges coupled with three dummy strain gauges for temperature compensation were used in three quarter-bridge configurations. The strain gauges were purchased from the company HBM, had a resistance of 120 Ω and were mounted inside the housing, shown in Figure 3.

The driver was equipped with a current transducer using the Hall effect from LEM (HAL 50-S). The sensor was capable of measuring RMS currents up to 50 A with frequencies from 0 kHz to 50 kHz. The current supplied to the DC-motor could thereby be measured and used for direct torque control (DTC) of the motor.

3. Calibrations

This chapter describes the calibration of the accelerometer, laser, inductive and current sensors and the strain gauges.

The accelerometer was mounted on a printed circuit board (PCB). The manufacturing calibration of this sensor, which assumes the accurate position of the accelerometer with respect to the x-, y- and z-axes, was not used, because it was mounted on the PCB with an angle with respect to those axes. For this reason, a lab calibration was carried out, as Figure 4 illustrates. The linearity between the acceleration and the voltage output in each direction, generated the following transfer functions:

$$G_x = \frac{X - 1.6285}{0.333} \tag{1}$$

$$G_y = \frac{Y - 1.6560}{0.333} \tag{2}$$

$$G_z = \frac{Z - 1.6665}{0.333} \tag{3}$$

where X, Y and Z are the voltage outputs in the x, y, z directions expressed in V; G_x , G_y and G_z are the values of acceleration in each direction with units of g; and 0.333 V/g is the sensitivity value of the accelerometer for the chosen operating voltage, according to the specifications of the sensor.

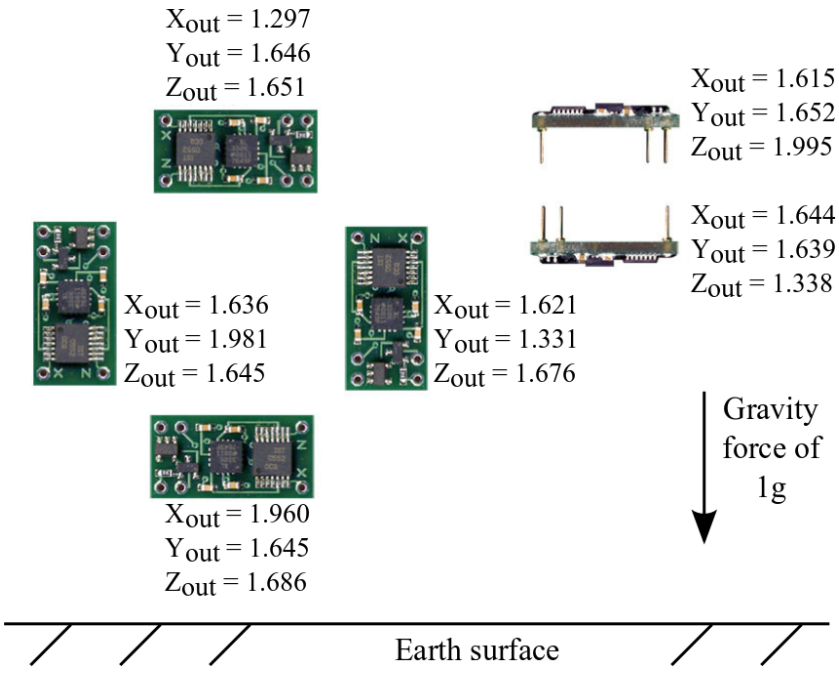

Figure 4. Calibration of the accelerometer in the x, y and z directions. The measurements are expressed in volts. The figure is based on [16].

The laser sensor was calibrated in the lab by using a tape measure and the head of the screw as a target. In Figure 3, a red dot can be seen underneath the screw head; that is, the laser beam spot hitting the target. The laser distance sensor outputs a value of current in the range from $4\,\text{mA}$ to $20\,\text{mA}$, and in order to obtain the calibration curve in Figure 5, a resistor of $220\,\Omega$ was used.

The transfer function for the laser sensor was found to be:

$$D = 50.85L - 20.5 \tag{4}$$

where D is the distance from the target in cm and L is the laser voltage output expressed in V.

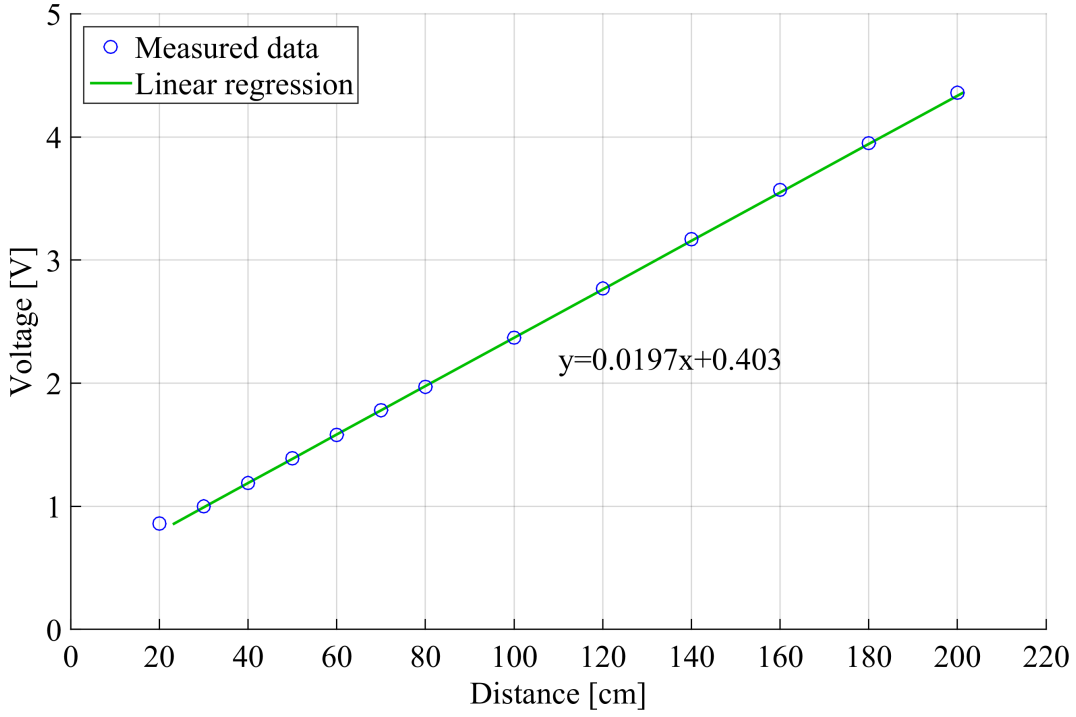

Figure 5. Calibration of the laser sensor. By inverting the linear regression equation, Equation (4) is found.

The inductive sensor was used to monitor the relative angular position of the motor. Two teeth of different sizes made of conductive material were mounted on the shaft; hence, every time the sensor registered two significant variations in voltage output, the control system translated them into one revolution of the shaft. Figure 6 shows seven revolutions of the shaft: it can be noticed how the size of the teeth reflects the width of the voltage variation.

In order to calibrate the strain gauges, the lower part of the screw was hooked to the barge where the buoy was resting, as can be seen from Figure 7a. In particular, as shown in Figure 7b, a dynamometer was placed along one edge of the sling, and then, the screw was slowly lifted upwards.

At each screw position, a different force was measured with the dynamometer, and a corresponding value of voltage was registered by the strain gauges. Knowing the geometry of the sling, the dynamometer reading was manipulated to obtain the value of force acting in the vertical direction. The amplification circuit of the strain gauges gave an output voltage range of $\pm 5\,\text{V}$.

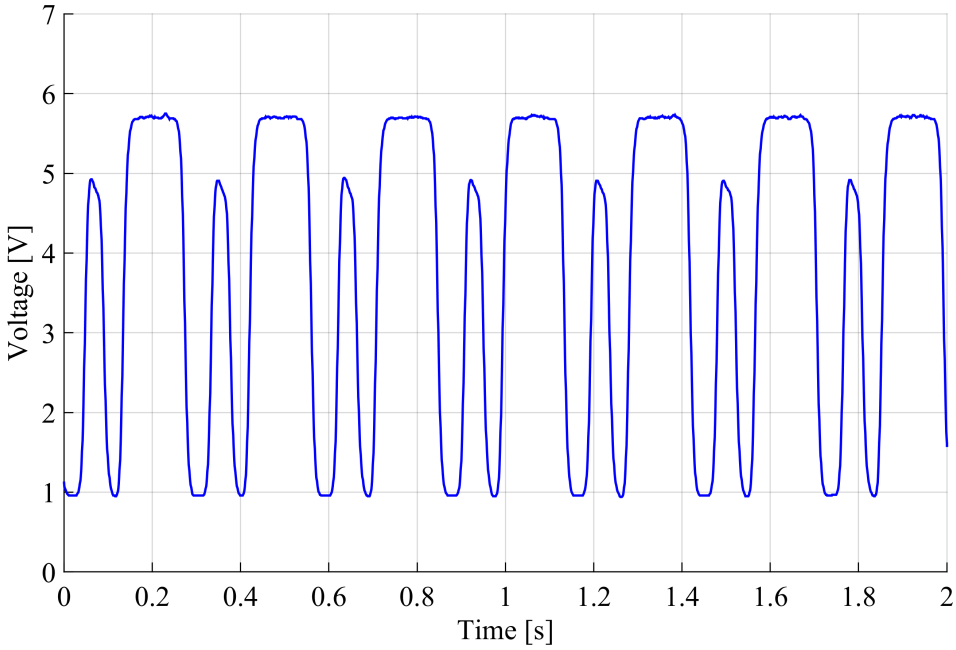

Figure 6. Calibration of the inductive sensor. The graph shows seven revolutions of the shaft of the motor.

(a) **(b)**

Figure 7. Calibration of strain gauges. (**a**) The buoy stored on a barge at the Lysekil harbor; (**b**) the screw was hooked to the barge via a lifting sling.

The calibration was repeated three times, and the calibration curves in Figure 8 were obtained. The regression line equations are:

$$y_1 = -0.01500x_1 \tag{5}$$

$$y_2 = -0.02002x_2 \tag{6}$$

$$y_3 = -0.02015x_3 \tag{7}$$

where y_i is the output voltage in V from the strain gauge i and x_i is the force in kN that produces that output. Considering that an error was introduced when reading the output of the dynamometer and when averaging the output from the strain gauges, the 95% confidence bands for the calibration lines were calculated and plotted. The joint distribution of the estimators for slope and intercept gives confidence bands having a hyperbolic shape.

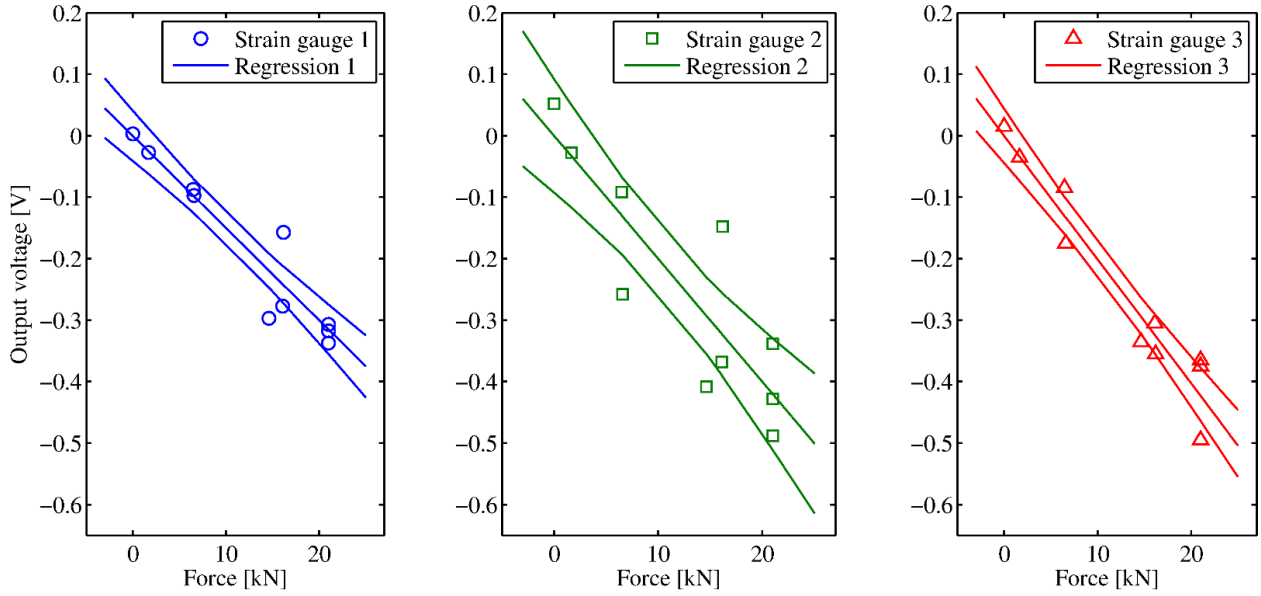

Figure 8. Calibration of the strain gauges. The graphs show the calibration lines for each strain gauge and their 95% confidence bands.

The motor that drove the screw jack was current controlled with a target level of 20 A. Hence, some tests were made to evaluate the necessary current required to lift a certain weight. In the same fashion as the strain gauges' calibration, the screw was pulled using different weights, and the minimum current required to lift them was measured. The result is shown in Figure 9, where the experimental data and the regression line of equation $y = 1.8x - 6.3$ indicate that a 20 A current control was sufficient to move the 2.7 t translator.

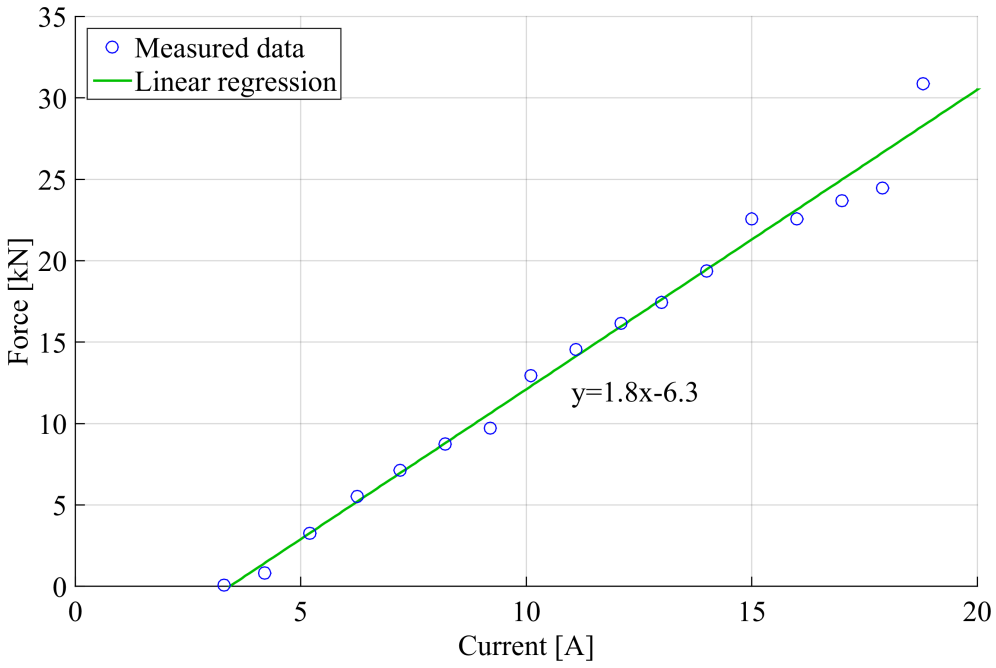

Figure 9. The graph shows the linear correlation between the pulling force applied to the mechanical device and the minimum current required to lift the screw.

4. Nearshore Test

4.1. Assembly and Deployment

The tidal compensation system was tested in the Lysekil harbor before its real deployment and connection to the L9 wave energy converter. The goals of the test were many: among others, to verify the self-locking feature and the correct dimensioning of the screw jack, to calculate the power consumption of the entire system when active, to compare the requested motor shaft revolutions with the performed revolutions and to monitor the screw position, to make sure that the exchange of SMS and the data transfer worked.

In order to do so, the buoy was assembled by bolting the lid on top of the housing and the lower tube underneath it; see Figure 10. Then, the buoy was lifted, and a weight of 2.5 t was hooked to the guiding line to simulate the weight of the translator; Figure 11a. The guiding line was connected to the screw (see Figure 10b,10c) and to the weight (see Figure 11a) via closed spelter sockets. Once the buoy was in the water and the crane slowly released the tension in the slings, the test was ready to begin.

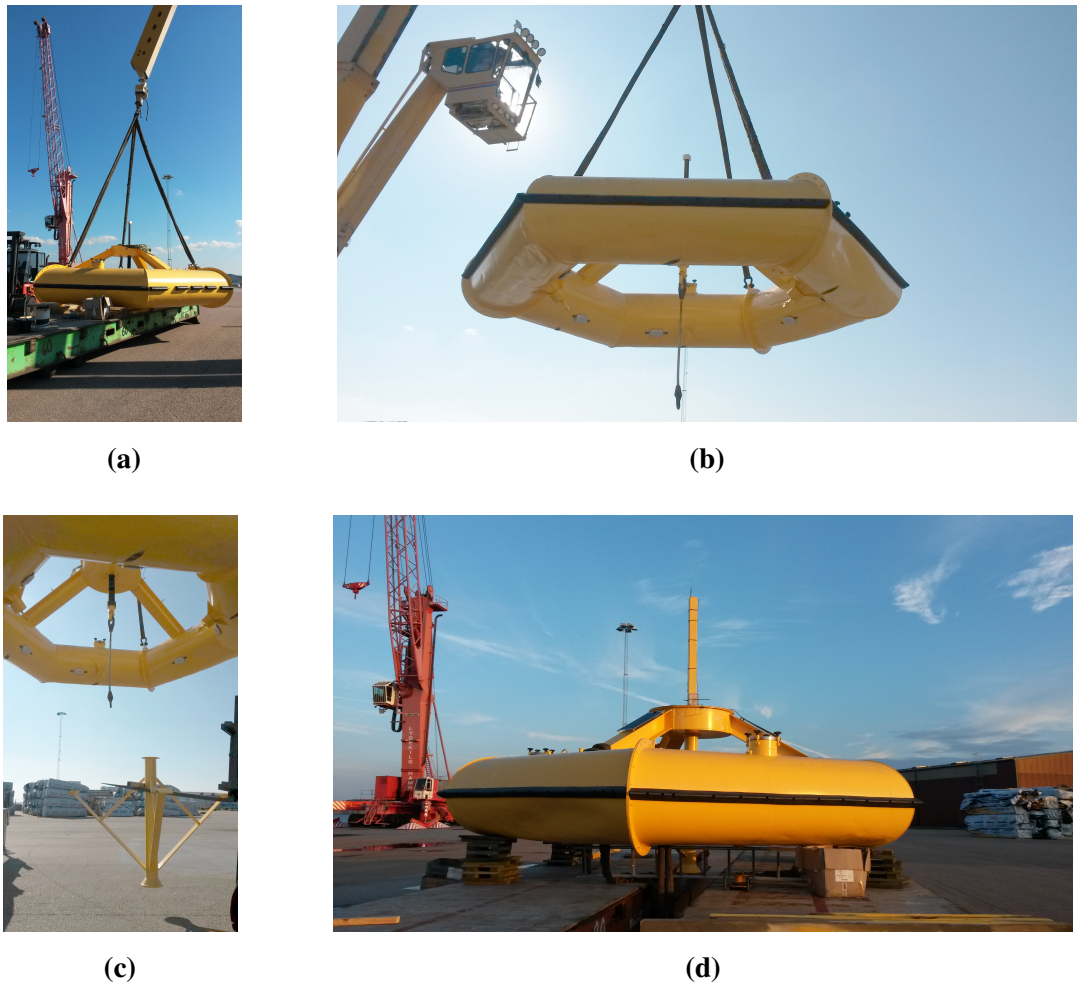

Figure 10. Pictures of the assembly. (**a**) A crane lifts the buoy; (**b**) the guiding line hangs underneath the screw; (**c**) the lower tube; (**d**) the buoy is placed on a barge, and the lid is mounted.

(a) **(b)** **(c)**

Figure 11. Pictures of the harbor test. (**a**) Concrete weights for a total of 2.5 tons; (**b**) solar panels visible on the lid and along the beams; (**c**) the crane releases the buoy and the test starts.

4.2. Results and Discussion

The test of the tidal compensation system was run on 22 October 2014, between 2 p.m. and 3 p.m. in the waters of the Lysekil harbor. As a first important result, the buoy having a total weight of approximately 5 t showed very good buoyancy, as can be seen in Figure 11c.

Once the buoy was in the water and the crane released the pulling force from the slings, the experiment started: a total number of five SMSs was sent to the buoy to adjust the position of the screw. The first three SMSs asked the motor to lower the screw 20 cm each time. The following two SMSs requested the screw to move upwards by the same amount. The last command was only partially executed because of the interruption of the test due to battery discharge.

This flow of commands is visualized in Figure 12, where the position of the screw changes according to the commands sent to the buoy. The screw moved downwards from 77.8 cm to 17.8 cm and, then, upwards to 55.9 cm. An adjustment of 20 cm was completed in approximately 5 min, independent of the direction of motion.

There was a time interval of about 6 min at the beginning of the test that corresponded to the buoy deployment, after which the adjustment started. Furthermore, there was a time interval of about 1 min between each screw adjustment: that was the time it took for the control system to send a feedback SMS and to receive the following SMS. During the nearshore test, the commands were manually sent from a personal mobile phone, while in the offshore operation of the buoy, the commands will be sent automatically via a telecommunications network facility called the SMS gateway, which allows a computer running a MATLAB script to send SMSs via email [13].

In order to calculate the power consumed by the motor, proportional to the angular velocity of its shaft, the derivative of the screw position calculated from the output voltage of the inductive and laser sensors was evaluated. Figure 12 shows that the position calculated by the two sensors was different at positions lower than 20 cm. This was due to the laser sensor going out of its specified range, which gave erroneous readings as a result.

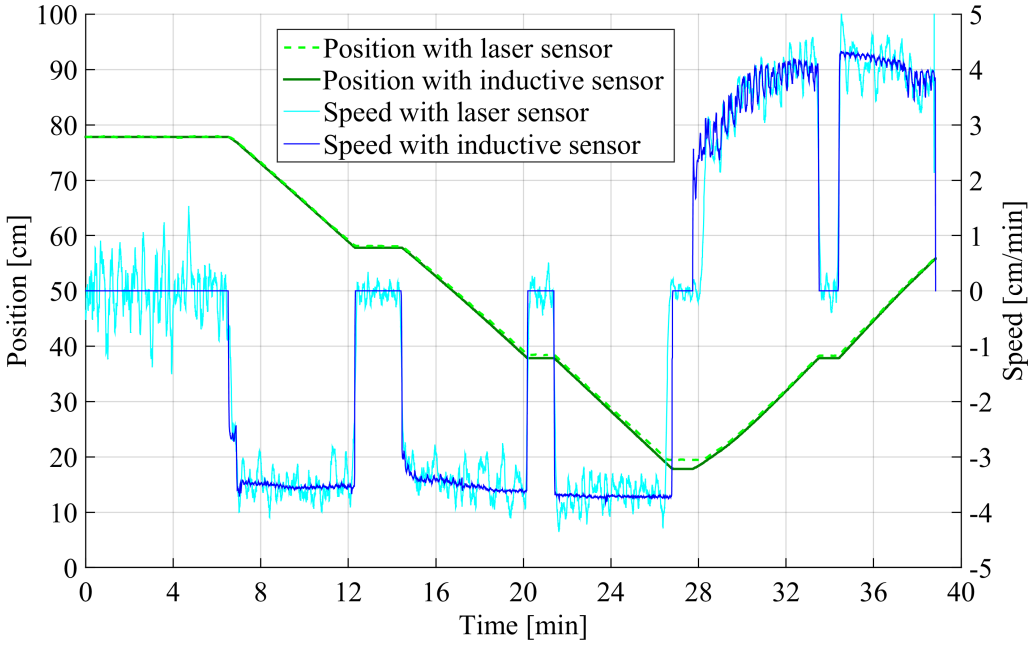

Figure 12. The position and the speed of the screw calculated from the inductive and laser sensor outputs.

An interesting result is the noise level of the speed calculated from each sensor output. The velocity obtained from the laser sensor is characterized by a noise level that is one order of magnitude higher than the one calculated from the output of the inductive sensor. Figure 12 shows it clearly, especially considering that the speed calculated with the laser sensor has been smoothed more heavily than the other one. For the application described within the paper, the use of the inductive sensor binary output gives better results than the output of the more expensive laser sensor.

Furthermore, the power consumed by the motor P_m was calculated using the formula:

$$P_m = \tau_m \times \omega_m \tag{8}$$

where τ is the torque and ω the rotational velocity. The subscript m refers to the motor. The corresponding power actually required to move the load, P_l, was evaluated as:

$$P_l = v_l \times F_l \tag{9}$$

where v_l is the linear velocity of the load and F_l the gravitational force of the load. The results of this evaluation can be found in Figure 13.

The power consumption during downwards motion had a peak of 194 W at the beginning of the test and a minimum of 140 W during the second adjustment, approximately. The low-frequency variations were probably due to differences in the lubrication of the screw at different positions and to the small waves moving the buoy during the test. The high-frequency variations were most likely due to noise in the current measurements and speed derivation. The power consumption during the upwards motion was in the range from 86 W to 230 W, approximatively. As mentioned before, the screw seemed to have trouble moving upwards the first time; but, after a low-speed transient, the velocity became constant, and the power reached a value of about 185 W between Minutes 30 and 33. The fourth adjustment showed a non-linear motion of the screw that is reflected in the power consumption plotted in black in the same

figure. The power consumption during the last adjustment was more constant, with an average value around 210 W.

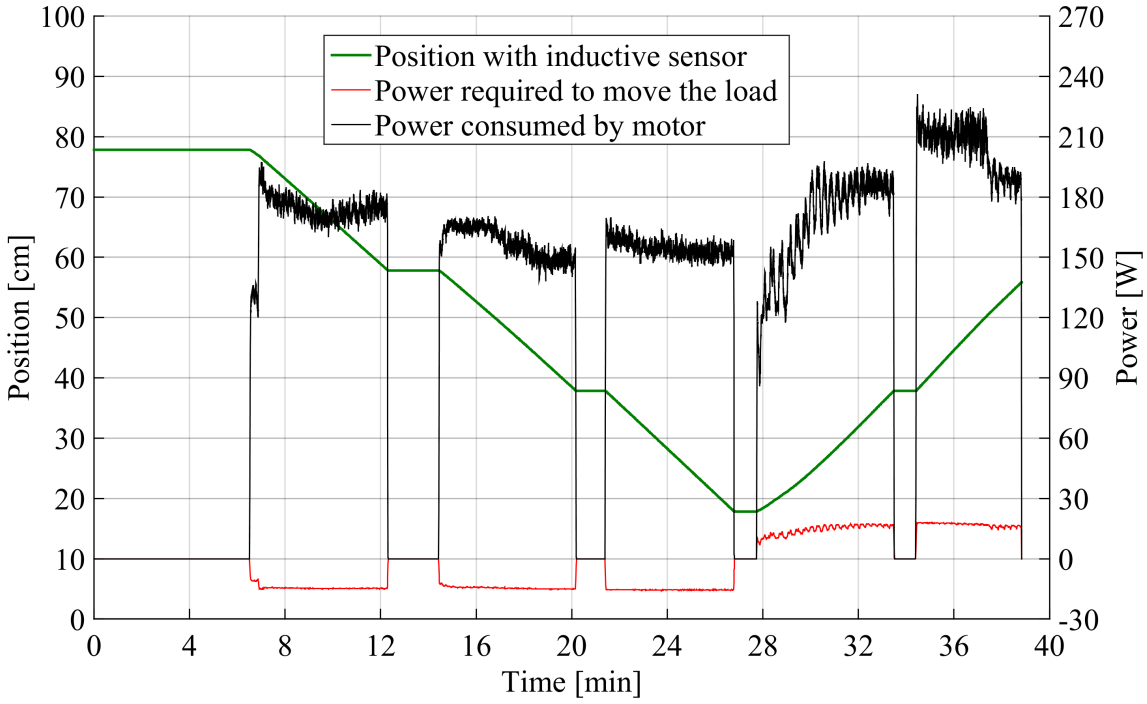

Figure 13. The position of the screw together with the power consumed by the motor, as well as the power required to move the load.

Moreover, Figure 13 illustrates the power that would be required to just move the screw in both directions, in order to estimate the frictional losses of the mechanical system. The negative part of the curve indicates that the motion of the screw was facilitated by the force of gravity: this is reflected in the power consumption, which is lower in the first three downwards adjustments and higher in the last two. The power consumed by the motor was about 10-times higher than the power required to lift the weight. This was due to the self-locking feature of the mechanical system, which typically makes the screw jack inefficient due to the high friction of the worm gear.

From Figure 13, it can be approximated that the linear actuator consumes 200 W during its motion, and it moves at a speed of about 4 cm/min. Assuming that the system has to compensate for a daily semi-diurnal tide of a maximum of 40 cm in Lysekil, the linear actuator has to move 1.6 m in total every 24 h.

The total energy demand of the linear actuator during one day is:

$$E_{actuator} = \frac{200\ (W) \times 1.6\ (m)}{0.04\ (m/min) \times 60\ (min/h)} = 133\ Wh \tag{10}$$

The standby losses, including control and measurement systems, were measured as 15 W in the current design, making the daily standby energy consumption equal to:

$$E_{standby} = 15\ (W) \times 24\ (h) = 360\ Wh \tag{11}$$

The total daily energy requirement of the system operating in Lysekil amounts to 493 Wh maximum. The same system could be used in offshore areas with higher tidal amplitudes, where the daily

semi-diurnal adjustment could reach 4 m; hence, the total energy demand of the linear actuator would rise to 333 Wh. In the latter case, using the two 12 V, 100 Ah, batteries connected in series, for a total of 2.400 Wh, the entire system could theoretically run approximately 3.5 days without charging.

A last comment should be given regarding the performance of the accelerometer and strain gauges. The accelerometer measurements were of negligible importance considering that the test was carried out in a harbor with very small waves. The strain gauges were calibrated before the final assembly, and the stresses applied on the buoy after the lower tube and the lid were mounted changed the zero reference of the gauges. The sensitive amplification circuit stopped working properly, and the voltage output from the strain gauges was considered unreliable.

5. Conclusions and Future Work

A tidal compensation system that allows wave energy generators to operate optimally in regions with tides has been constructed and subjected to nearshore tests. A detailed description of the electro-mechanical, control, communication and measurement systems has been presented down to the article numbers of installed equipment and calibration curves. The operational energy and power requirements of the compensation system are presented, showing, as expected, the relatively low energy efficiency of the system (a consequence of a simpler mechanical design where the need for a locking system has been avoided). The results show that the level of the standby energy consumption of the device, which is the dominant energy sink of the system during daily operations, allows the buoy to function properly during the summer. The power collected by the solar panels is, however, not enough to cover the energy requirements during the dark Swedish winters. Future work will show the buoy in operation with a wave energy converter, as well as efforts to lower the energy requirements of the system.

The nearshore test described within the paper had the important value of verifying the prototype design of the buoy, of helping identify problematic design areas and of highlighting potential improvements to the system. The areas to which priority has to be given are presented below, as well as solutions that could be adopted.

5.1. Energy Harvesting and Consumption

Arguably, the most critical problem in the current design is the inability for the system to perform daily tidal compensation during winter in the Northern Hemisphere. The offshore test of the tidal compensation system was planned to take place in the summer and for a limited period of time. This led to the choice of solar panels to charge the batteries. Of course, a different solution has to be proposed for the future offshore operation of the system. Three potential solutions to this problem will be presented below.

The first solution is to increase the amount of stored energy by using more batteries or batteries with higher energy density. However, this poses another issue: the amount of energy storage required to last the whole winter is simply too large, making any solution, like the use of high-end lithium batteries, both impractical and expensive.

The second solution is to increase the amount of collected energy by increasing the amount of solar panels or installing alternative energy collectors, such as wind turbines. The use of a small-scale wind

turbine is considered one possible solution. In fact, increasing the buoy area covered with panels would have little effect on the battery charging in parts of the world where the sunlight is much weaker during winter time. On the contrary, wind is usually plentiful at sea all year around. A wind turbine that could replace or be integrated with the solar panels is the LE-300 from Leading Edge [19]. Assuming a mean wind speed of about 5 m/s at 2 m above the water surface, this turbine would generate 25 W, generating a total of 600 Wh during 24 h. However, the harsh offshore environment could compromise the life time of the wind turbine. Experience gained from the experiments carried out at the Lysekil research site tells us that anything closer than 4 m to the water surface is exposed to potentially harmful waves. The alternative would be to focus on a different types of energy collectors, such as oscillating energy harvesting systems, which extract power from the oscillations of the buoy [20]. This kind of solution will require proper dimensioning and testing, in order to make sure it will provide the required power.

The third solution is to reduce the energy requirement of the system by using a more efficient linear actuator, replacing the over-dimensioned motor driver and reducing the standby losses. However, redesigning the linear actuator is deemed to expensive and not very effective considering that the actuator is supposed to be inefficient because of its self-locking feature. Therefore, most work will be put into reducing the other losses. A reduction from the present 15 W to 5 W could potentially save 240 Wh a day, a reduction of 50% of the total energy requirement. Part of the losses are generated by the motor driver, which was over-dimensioned to ensure reliability. The alternative is to use a commercial-off-the-shelf product, like the TYP4 motor controller from Sepro [21], which will decrease the power consumption and guarantee equally good performance. However, most of the losses are generated by the standby components, like the cRIO, an excessively power consuming device for the present application, and the RPi, which consumes about 2.5 W, even though it does not have high computational power. An alternative would be to replace both the cRIO and RPi with more power-efficient devices. The new setup could include the A20-OLinuXino-LIME from OLIMEX, a device which uses similar technology as the one found in modern smart phones [22]. It offers more than four-times the computational power of the RPi, and it consumes less power. The A20 has a standby power consumption of about 1.1 W [23]. The measurement system sensors could be directly interfaced towards the A20. However, in order to replace the time-critical tasks of the cRIO, such as generating PWM pulses for the motor driver, additional hardware is required, e.g., a small micro-controller connected to the A20 through USB. For example, the ATmega328P micro-controller made popular by the Arduino [24]. Typically micro-controllers of this class have a power consumption in the order of 0.1 W. Many other less-known micro-controllers can be found on the market, like the Teensy 3.1 from PJRC [25]. Together, these improvements could drastically reduce the standby losses.

5.2. Strain Gauges Amplification Circuit

A problem with the current setup is the unreliability of the strain gauges. These do not play a vital role during the operation of the buoy itself or the tidal compensation system. Instead, they are used to collect valuable data of the mechanical loads in the buoy structure. In the current system, the gauges need a physical calibration: various potentiometers have to be manually adjusted on the amplification board mounted inside the buoy. Once the Wheatstone bridge is calibrated on shore, there is no possibility

to make any change after the buoy is deployed. Once again, a commercial off-the-shelf solution is considered the best way of improving the system. The use of the USB-powered strain gauge amplifiers is suggested, such as the DSCUSB from Mantracourt [26] or the SY047 digital amplifier from SYNECTIC ELECTRONICS [27]. These amplification circuits will simplify the calibration procedure and increase the reliability of the output from the strain gauges.

Acknowledgments

Thanks go to the Swedish Energy Agency, Ångpanneföreningen, STandUP for Energy and the Carl Triggers Foundation for their financial support.

Author Contributions

Valeria Castellucci contributed extensively to the work described in this paper by designing, building, preparing and running the experiment. She was responsible for the data acquisition, analysis and drafting the article. Johan Abrahamsson contributed to the design of the control system, gave technical support during the preparation of the experiment and participated in the data analysis. Tobias Kamf helped during the laboratory tests of the system and gave suggestions for future work. Rafael Waters conceived the project, supervised it and gave the final approval. All of the co-authors participated in writing the paper.

Conflicts of Interest

The authors declare no conflict of interest.

References

1. Leijon, M.; Boström, C.; Danielsson, O.; Gustafsson, S.; Haikonen, K.; Langhamer, O.; Strömsted, E.; Stålberg, M.; Sundberg, J.; Svensson, O.; *et al.* Wave Energy from the North Sea: Experiences from the Lysekil Research Site. *Surv. Geophys.* **2008**, *29*, 221–240.
2. Tyrberg, S.; Waters, R.; Leijon, M. Wave Power Absorption as a Function of Water Level and Wave Height: Theory and Experiment. *IEEE J. Ocean. Eng.* **2010**, *35*, 558–564.
3. Eriksson, M.; Waters, R.; Svensson, O.; Isberg, J.; Leijon, M. Wave power absorption: Experiments in open sea and simulation. *J. Appl. Phys.* **2007**, *102*, doi:10.1063/1.2801002.
4. Boström, C.; Lejerskog, E.; Tyberg, S.; Svensson, O.; Waters, R.; Savin, A.; Bolund, B.; Eriksson, M.; Leijon, M. Experimental results from an offshore wave energy converter. *J. Offshore Mech. Arct. Eng.* **2010**, *132*, doi:10.1115/1.4001443.
5. Waters, R.; Stålberg, M.; Danielsson, O.; Svensson, O.; Gustafsson, S.; Strömstedt, E.; Eriksson, M.; Sundberg, J.; Leijon, M. Experimental results from sea trials of an offshore wave energy system. *Appl. Phys. Lett.* **2007**, *90*, doi:10.1063/1.2432168.
6. Tyberg, S.; Svensson, O.; Kurupath, V.; Engström, J.; Strömsted, E.; Leijon, M. Wave Buoy and Translator Motions—On-Site Measurements and Simulations. *IEEE J. Ocean. Eng.* **2010**, *36*, 377–385.

7. Castellucci, V.; Waters, R.; Eriksson, M.; Leijon, M. Tidal Effect Compensation System for Point Absorbing Wave Energy Converters. *Renew. Energy* **2013**, *51*, 247–254.
8. Castellucci, V.; Abrahamsson, J.; Svensson, O.; Waters, R. Algorithm for the calculation of the translator position in permanent magnet linear generators. *J. Renew. Sustain. Energy* **2014**, *6*, doi:10.1063/1.4900553.
9. For Info on Solar Panels. Available online: https://www1.elfa.se/data1/wwwroot/assets/datasheets/CTsolarmarine_eng_tds.pdf (accessed on 11 December 2014).
10. For Info on the Regulator. Available online: http://www.clasohlson.com/se/Batteriregulator/36-4452 (accessed on 7 January 2015).
11. Ekergård, B. Full Scale Applications of Permanent Magnet Electromagnetic Energy Converters. Ph.D. Thesis, Uppsala University, Uppsala, Sweden, 2013.
12. Boström, C. Electrical Systems for Wave Energy Conversion. Ph.D. Thesis, Uppsala University, Uppsala, Sweden, 2011.
13. Castellucci, V.; Eriksson, M.; Waters, R.; Ferhatovic, S.; Leijon, M. Wireless System for Tidal Effect Compensation in the Lysekil Research Site. In Proceedings of the 31st International Conference on Ocean, Offshore and Arctic Engineering (OMAE2012), Rio de Janeiro, Brazil, 1–6 July 2012.
14. For Info on the GSM Modem. Available online: http://www.induowireless.com/wp-content/uploads/2014/03/maestro-100-maestro-20.pdf (accessed on 11 December 2014).
15. For Info on the Raspberry Pi. Available online: http://www.raspberrypi.org/products/model-b-plus/ (accessed on 11 December 2014).
16. For Info on the Accelerometer. Available online: http://www.dimensionengineering.com/datasheets/DE-ACCM3D.pdf (accessed on 11 December 2014).
17. For Info on the Laser Sensor. Available online: http://www.micro-epsilon.co.uk/download/products/cat–optoNCDT-ILR–en.pdf (accessed on 30 January 2015).
18. For Info on the Inductive Sensor. Available online: http://www.farnell.com/datasheets/33697.pdf (accessed on 11 December 2014).
19. For Info on the Wind Turbine. Available online: http://www.leturbines.com/wp-content/uploads/2013/10/LE-300-brochure-web-version-311013.pdf (accessed on 9 February 2015).
20. Elmes, J.; Gaydarzhiev, V.; Mensah, A.; Rustom, K.; Shen, J.; Batarseh, I. Maximum Energy Harvesting Control for Oscillating Energy Harvesting Systems. In Proceedings of the Power Electronics Specialists Conference, Orlando, FL, USA, 17–21 June 2007.
21. For Info on the Motor Controller. Available online: http://www.seproab.se/Filer/pdfer/TYP4_produktblad_en.pdf (accessed on 12 February 2015).
22. For Info on the A20-OLinuXino-LIME. Available online: https://www.olimex.com/wiki/A20-OLinuXino-LIME#Linux (accessed on 12 February 2015).
23. For Info on the A20-OLinuXino Power Consumption. Available online: https://www.olimex.com/Products/OLinuXino/_resources/OLinuXino-Consumption.pdf (accessed on 12 February 2015).
24. For Info on the Arduino. Available online: http://arduino.cc/en/Main/ArduinoBoardNano (accessed on 12 February 2015).
25. For Info on the Teensy 3.0. Available online: https://www.pjrc.com/teensy/ (accessed on 12 February 2015).

26. For Info on the Amplification Circuit From Mantracourt. Available online: http://www.mantracourt.com/products/signal-converters/usb-load-cell-converter (accessed on 12 February 2015).
27. For Info on the Amplification Circuit From Synectic. Available online: http://www.synectic.co.uk/weighing/load-cell-amplifier/sy047-dual-channel-digital-loadcell-amplifier.html (accessed on 12 February 2015).